A Self-Referenced Hand-Held Range Sensor

Patrick Hébert
Computer Vision and Systems Laboratory
Laval University, Québec, Canada
hebert@gel.ulaval.ca

Abstract

Due to its portability and great maneuverability, a hand-held range sensor is a flexible solution or complement to efficiently digitize the 3-D shape for a wide variety of objects. This paper firstly presents a review of the existing hand-held technologies. Although the designation encompasses various system configurations, the structured light pattern, if any, and sensor positioning are key elements. A trinocular configuration with two synchronized cameras and a light pattern projector is then proposed and tested experimentally. To eliminate the necessity for an external positioning device, a set of points are projected in the scene using a fixed and independent projector. The proposed configuration reveals interesting characteristics for calibration and measurement robustness.

1. Introduction

There is currently a very strong need for building 3-D models of the visible surface for a wide variety of objects in shape, size and type of material. Applications require to inspect, document, reproduce, or simply provide the capability to remotely observe the representation of a real object under any selected viewpoint. Reducing data collection and modeling time as well as developing more flexible systems that are portable, simple and easy to use now become a necessity.

A hand-held range sensor is a useful tool in many situations. Since it is maneuverable, it is easy to select the area to be measured without the constraint on motion imposed by a translation or rotation system. It is also easy to orient the sensor relative to the surface to get the optimal coverage (sampling) or the optimal conditions for measurement quality. When a hand-held sensor is coupled to a positioning system, the number of surface patches that must be manually integrated to recover a partial or complete model of an object, is significantly reduced. Nevertheless, a hand-held sensor is not a panacea. Depending on the size of the object and the model quality requirements, it can be more advantageous to use a hand-held sensor only as a complementary tool to measure areas of the object that cannot or, more difficultly, be measured using a displacement system. (see [1] for a convincing application).

This paper has two objectives. We present a review of the current hand-held system technologies. Then, a new sensor for locally measuring the geometry of an object is proposed; the sensor is based on structured light projection. The sensor has not only the advantage of being simple and robust but it integrates both the shape measurement and self-referencing.

After a review of the current hand-held technologies, the proposed system architecture is presented. The main aspects including sensor calibration, self-referencing, image processing and 3-D point computing are described in the following sections. To demonstrate the feasibility of the proposed system, each section includes experimental results.

2. Previous work

As long as the light integration time is short enough with respect to the displacement of the sensor, it is possible to avoid motion blur within a single frame and use a range sensor hand-held provided it is compact enough. EOIS [2] and Minolta [3] are examples of companies commercializing such sensors. In both cases, a 2D pattern of light (full field) is projected on the object. While the former is a Moiré based sensor with a working volume of $200 \times 200 \times 120$ *mm*, the later is built on a standard digital camera coupled to an adapted flash projecting a structured light pattern. This last sensor is appropriate for objects from 100 to 400 *mm* in size at a distance between 500 to 900 *mm*. The Virtuoso sensor developed at Visual Interface exploits 6 cameras to observe a projected pattern [5]. This sensor has been used by the IBM research team [4]. Using one of these hand-held full field sensors, a set of 3D frames can be captured and merged by software and manual alignment. In this case data collection is independent to data integration.

To better integrate data from different viewpoints, it is interesting to attach these sensors to a positioning device

that will provide the transformation between a mobile coordinate system and a global fixed coordinate system. By calibrating the additional "hand-eye" transformation, data collected by the sensor can be transformed from the sensor coordinate system to the global coordinate system. It is then essential that every 3-D frame be synchronized with the positioning system.

There are various types of positioning devices including mechanical, electromagnetic, acoustic, optical and inertial.

Mechanical arms can be very accurate relative to the working volume. For instance, the 1,2 *m* Gold Faro arm [6] can measure a 3-D point by contact within 25 microns (2σ). 3dScanners [7] and Kreon Industries [8] are examples of companies offering a laser profile range finder that can be mounted on a mechanical arm. We have also experimented for several months using a similar system where a Biris range profile sensor was mounted on a mechanical arm [9]. We realized the limitation imposed by the mechanics when it was necessary to move around an object. For small objects, these arms are advantageously used in combination with a turn table.

Electromagnetic sensors offer more freedom of motion but less accuracy. They are significantly sensitive to the presence of metal objects. Although this type of positioning device was used in [10][11], the "FastScan" distributed by Polhemus and initially developed by Industrial Research is probably the best known [12]. The range profile sensor is composed of two cameras at the extremities of a 450 *mm* wand along with a laser plane projector set in the center. The transmitter is fixed, though eventually attached to a moving object, and the receiver mounted on the wand. The sensor outputs 50 lines/s with a standoff distance of approximately 200 *mm* and the transmitter range is approximately 700 *mm*. According to the specifications, the accuracy would be in the order of 1 *mm*.

Acoustic and optical devices are interesting alternatives. In this last case, LEDs can be fixed to the sensor and tracked by cameras mounted on a fixed base [13]. One must then make sure the sensor is always kept in the field of view. Intertial systems combining gyroscopes and accelerometers have been used in photogrammetry [14]. If the drift becomes negligible and the sensor accurate enough, this could be a promising alternative.

Eliminating the positioning device would be desirable. This can be made possible if the sensor could reference itself *from the observation*. Important effort in this direction has been made in the case of a passive uncalibrated video camera [15]. The detection of natural landmarks, the precision of their positions and the complex correspondence problem are challenging issues. Roth and Whitehead [16] address this problem in the perspective of eventually combining passive positioning and active sensing. A different approach consists in placing 2-D or 3-D reference targets in the scene [17]. An example of a 2-D pattern used to position a passive camera in a shape-from-silhouette approach is described in [18].

A different class of hand-held range sensors has been proposed in the perspective of reducing the complexity of a system. Since an active range sensor is usually composed of an illuminant and a photosensor (camera), it is possible to keep the later fixed and manually control the illuminant to scan an object. For instance, Bouguet and Perona [19] used a calibrated camera mounted on a tripod. They also calibrate a plane of reference on which the object can be set. Using a simple desk lamp as a fixed point source of known position, they scan the scene using a rod projecting a shadow on the object as well as on the reference plane. When the light source position is not known, they can exploit the intersection of the shadow with a second calibrated plane usually perpendicular to the first plane. These planes must always be visible. Although they demonstrate the feasibility for large objects, it is more appropriate for small objects. Immersion [20] commercializes an adaptation where small objects (< 300 *mm*) are set on a rotation table with a backplane. In this case, the technique is complementary to a shape-from-silhouette approach where it allows for eliminating ambiguities due to concavities. The illuminant pattern is a laser line projector that can be moved hand-held.

To avoid using planes of reference that must always be visible, Fisher *et al* [21] have modified the initial idea of [19] by using a custom rod whose profile is a triangle of known dimensions and including two positioned marks. This makes it possible to estimate the intersection of the shadow and the object using a calibrated fixed camera provided the source is fixed. The idea is interesting for objects that cannot be displaced or where it is not possible to install planes that must be visible in the image.

Takatsuka *et al* [22] also use a fixed calibrated camera and a hand-held laser point projector on which 3 green LEDs are fixed along the optical axis of the laser. During scanning, the 3-D coordinates of the 3 points are computed from their 2-D image coordinates to determine the optical axis of the laser. The 3-D coordinates of the projected point on the object is estimated as the intersection of the viewing direction of the camera and the laser axis. The "Autoscan" system [23] uses instead two cameras mounted on a tripod and a hand-held laser point projector. With a baseline of 1 m and a standoff distance of 1,5 *m*, measurements are captured at 100 Hz with an accuracy of 0,1 *mm*.

These systems are simple but they are all fundamentally limited to a single view. Using a rotation table for small object is an interesting complement since view integration has only to be performed for the top and bottom views.

3. The proposed architecture

Our objective is to develop a sensor that can be easily deployed on site and that has the potential to produce accurate measurements. It uses structured light to capture dense measurements. The hardware is simple and the emphasis is put on close software integration.

The proposed architecture is an active triangulation based sensor where both the laser illuminant and the sensing area are rigidly integrated. To improve freedom in motion while avoiding an external positioning device, the sensor is self-referenced from observations. The measurable surface is thus not fundamentally limited to a fixed view. In order to position the sensor in a global coordinate system, a set of fixed points are projected on the visible surface. The first advantage is that no physical target has to be put on the object to be measured. A second advantage is the possibility to project a set of points on a selected area. For the same reasons a light pattern is projected on the surface to be measured, these fixed points facilitate correspondence for the positioning of the mobile camera. Both the reference and the shape measurements are integrated. Positioning measurement is thus inherently synchronized and there is no need to calibrate an external transformation with respect to a positioning device.

Besides these advantages, the selection of a crosshair pattern is motivated by the potential of improving surface shape estimation through rigid pattern registration. While the crosshair can be extracted easily using the proposed sensor configuration, more stable registration compared with simple profiles is possible [24].

Figure 1 depicts the active stereo (trinocular) configuration. The configuration integrates two synchronized cameras and one laser diode projecting two perpendicular light planes, a and b respectively. The trinocular geometry is compact for a given baseline. Other trinocular configurations have also been proposed for active range sensing

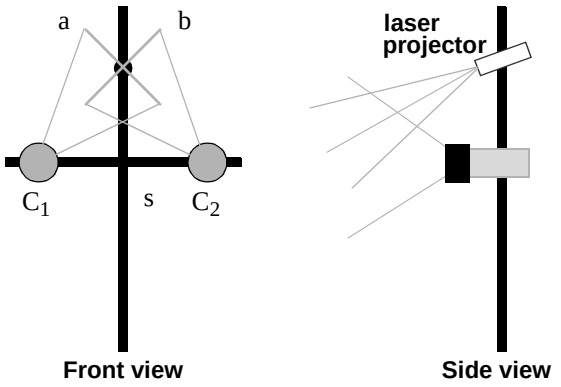

Figure 1. Trinocular sensor configuration: Two cameras and a crosshair light projector. The fixed point projector is not depicted.

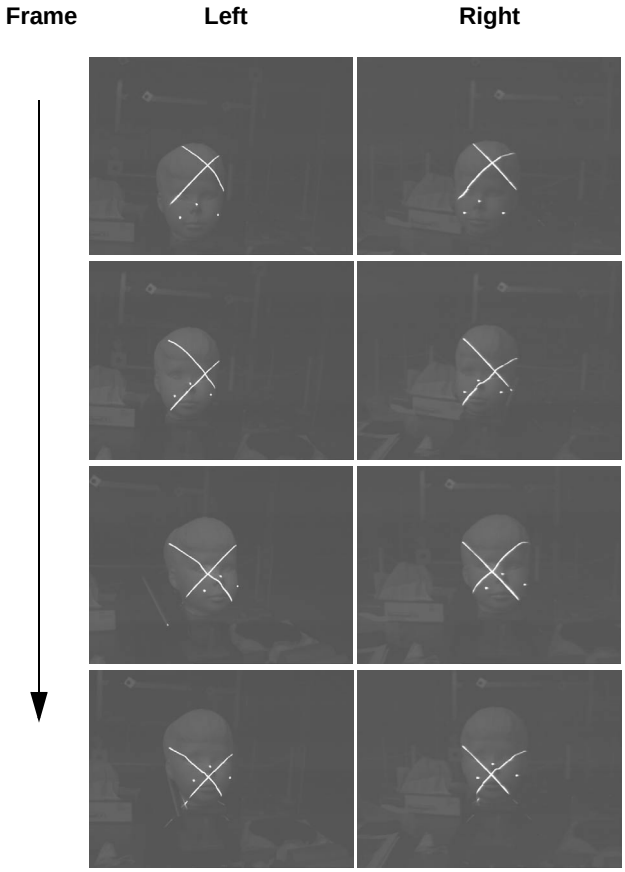

Figure 2. Four stereo frames illustrating the crosshair motion with respect to the fixed points.

[25][26]. In our case, the sensor is exploited as three cooperating sensors of which two are active. While the left sensor (in the Figure) is based on the combination of camera C_1 and plane a, the right sensor is based on plane b and camera C_2. The two cameras compose a passive stereo pair to observe reference points for positioning. The discrimination between the two projected planes in the images, is simple. Actually, cameras C_1 and C_2 are positioned such that one of the two light planes is projected near the principal point of the image. This causes a projected straight line at constant angle in the image plane and thus simplifies pattern detection. We refer to this plane as the *inactive* plane. It is used to validate a 3-D point computed from the opposite image. While in image C_1 plane b is the inactive plane, it is active in the right image C_2. Finally, the cameras and the laser projector are oriented such that the laser trace is always visible within the working volume.

The four stereo frames in Figure 2 illustrate the principle with three fixed points as well as the moving crosshair used to scan the object. A set of points can be projected on a larger area of the object and more projectors could be used to cover areas not seen from a single projector.

To demonstrate the feasibility, a sensor prototype is devised to capture measurements at a standoff distance of 400 *mm*. Focal lengths (F) of 6 *mm* are used to provide a wide field of view (70 degrees with 1/2 inch CCDs). From the equation

$$\sigma_z \approx \frac{z^2}{FD}\sigma_p\,, \tag{1}$$

a baseline (D) of 170 *mm* should conservatively lead to an expected uncertainty of $\sigma_z = 0,26mm$ in the sensor coordinate system (σ_p is the uncertainty in point position). The next sections describe the main steps to develop and experiment with the sensor.

4. Sensor calibration

The sensor calibration objective is twofold. First, both intrinsic and extrinsic parameters of the stereo pair are computed. Second, the equations of the two light planes are estimated in the stereo coordinate system. For improved robustness, the limits of the light planes are also determined and included in the sensor model. For each plane, these limits are 4 straight lines in the stereo coordinate system: the far and near limits of the working volume as well as the lateral limits.

There are several calibration methods and we observe in the literature that there is still intense research in this area. New methods are developed to improve accuracy, simplify usage, or reduce hardware costs of implementation. The sensor configuration makes it possible to use an accurate and very simple method to apply, which however requires a calibration target made of a plate with rods of different lengths. This calibration target is accurately measured beforehand using a CMM.

From a single stereo frame of the calibration target, the model parameters for the two cameras are estimated [27]. The relevant equations are

$$x - x_0 + dx = -f\frac{(X-X_0)m_{11} + (Y-Y_0)m_{12} + (Z-Z_0)m_{13}}{(X-X_0)m_{31} + (Y-Y_0)m_{32} + (Z-Z_0)m_{33}} \tag{2}$$

and

$$y - y_0 + dy = -f\frac{(X-X_0)m_{21} + (Y-Y_0)m_{22} + (Z-Z_0)m_{23}}{(X-X_0)m_{31} + (Y-Y_0)m_{32} + (Z-Z_0)m_{33}}, \tag{3}$$

where $m_{ij}(i,j = 1,2,3)$ are elements of the camera rotation matrix; X, Y, and Z are the coordinates of an observed point in 3-D space; x and y are the corresponding image coordinates; X_0, Y_0, and Z_0 are the camera projection center coordinates; x_0 and y_0 are the principal point coordinates; and f is the distance between the camera projection center and the image plane. The expressions for the distortion parameters, dx and dy, are

$$dx = a_1y' + x'(a_2r^2 + a_3r^4) + a_4(r^2 + 2x'^2) + 2a_5x'y' \tag{4}$$

and

$$dy = a_6y' + y'(a_2r^2 + a_3r^4) + a_5(r^2 + 2y'^2) + 2a_4x'y'\,, \tag{5}$$

where r is the radial distance from the image point to the principal point, $x' = x - x_0$, $y' = y - y_0$, a_1 and a_6 correct for affine scale and eventually compensate for imperfect perpendicularity of image axes; a_2 and a_3 are for radial lens distortion; a_4 and a_5 are for decentering lens distortion or non perpendicularity of optical axis to the image plane.

For 25 rods varying in length over a range of 200 *mm*, the parameters are estimated for both cameras. The target coordinate system defines the stereo coordinate system R_s. The X, Y, and Z coordinates for each target are computed from stereo and compared to the object. The standard deviations of the errors are (in *mm*):

$$\sigma_x = 6,56\times10^{-2}\ \ \sigma_y = 6,56\times10^{-2}\ \ \sigma_z = 0,268\ \cdot \tag{6}$$

The images of the target are displayed in Figure 3.

The next step consists in estimating the parameters of the two light planes produced by the laser crosshair projector in R_s. This can be done by capturing stereo frames of a planar object from at least two different positions delimiting the working volume. To ensure the best measurement quality, the observation is preferably made with the sensor observation axis nearly aligned with the plane normal. For each observation, the equations of the two projected lines in 3-D along with their estimated limits are computed. This is done by firstly fitting lines in the image plane (after compensating for distortion if necessary). For each of the two lines in the left image, two points are selected at the extremities. Then, one can exploit the fundamental matrix to identify the 4 corresponding points in the right image where the four epipolar lines intersect the two observed lines of the crosshair shape. From the stereo correspon-

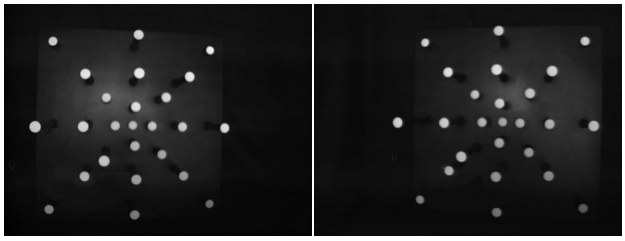

Figure 3. Stereo frame of the calibration target.

dences, the 3-D points are computed and used to fit the two planes in 3-D.

In most of our calibration experiments with this system, the sensor was held fixed on a tripod and the plane positioned by hand in fixed position. To assess the measurement error, we calibrated the laser planes more systematically using a translation stage where a planar object was moved over 300 *mm* by step of 5 *mm*. At each position, 3-D points were computed. The two planar regressions led to an estimated variance of $1,76 \times 10^{-2} mm^2$ along the normal of the 2 light planes. Except in this last scenario, the complete sensor calibration procedure can be done in less than 15 minutes.

5. Self-referencing

The sensor position is estimated in a global coordinate system from a set of points projected in the scene. For this purpose we use a fixed laser point projector whose position is not calibrated. To improve robustness to ambient lighting, interference filters can be used if the laser wavelength is the same as the sensor projector. Since we benefit from the stereo configuration, the minimal number of points to be matched is only 3 when no constraint is imposed to the camera motion. Increasing the number of points will improve accuracy and precision; it will also make it possible to cover a larger area to be scanned for a given fixed coordinate system. The trade-off is obviously the matching complexity. The feasibility is here demonstrated using 3 points.

The point projector is set to project points in the middle of the observed area such that points are visible from any sensor viewpoint of interest. In order to avoid symmetries, the projector is roughly oriented such that the triangle defined by the three points is not equilateral. There are three steps to estimate the sensor position: *i)* matching in the stereo frame to obtain a first set of 3-D points, *ii)* matching between the current 3-D point structure and the model built from previous frames, and *iii)* estimating the rigid transformation between the current sensor frame and the global coordinate system. The observed structure of the three points is also updated after each observation. This last step is related to the well known problem of structure and motion. The procedure is described in the next paragraphs.

Since there might be noise and the point detection may not be perfect, there are usually more than 3 points that are detected in each image. Typically, the number of points is less than 10. They commonly arise in the projected pattern. Although the number of points is low compared with typical passive stereo matching, this number is further reduced by imposing that the corresponding points in the left and

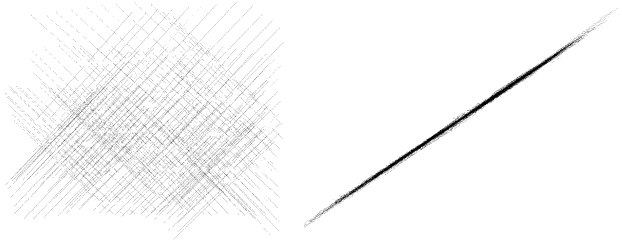

Figure 4. Measurement in a planar section along with a cross-section showing the planarity (24805 points).

right images lie on the respective epipolar lines (after distortion correction). Besides the epipolar constraint, it is further imposed that the estimated 3-D point in the stereo coordinate system be within the working volume of the passive stereo pair. The result is a small set of 3-D points in the stereo coordinate system.

The next step consists in matching the 3-D set of points with the model representation of the reference triangle accumulated from the previous frames. Among the combinations of pairs of 3-D points, the Euclidean distance is calculated and pairs for which this distance matches one of the three sides of the reference triangle, are identified as potential candidates for matching. A graph of these potential combinations is built where each point is a node and a link between two nodes is set when the combination is a candidate. The set of 3-cycles is found in this graph. From this set, each 3-cycle is matched to the referenced triangle based on their distances. The sum of the difference of distances for each ordered cycle is computed. The minimal cost loop is identified and kept provided, the difference in distance is within a threshold (a percentage of the triangle perimeter) and provided the 3-D order constraint is met. This last constraint ensures that the sensor has observed the points from only one side of the surface.

For a validated match, the rigid transformation that minimizes the squared error between the two matched triangles is computed:

$$\min_{R,\,T} \quad \sum_i (Y_i - RX_i - T)^2 . \qquad (7)$$

In this equation Y_i is a reference point and X_i is the corresponding observed point. The computed transformation will then be applied to the extracted points from the crosshair. When the basic point structure cannot be observed, the frame is discarded. Using only three reference points, this may happen where one or more points interfere with the crosshair pattern. Following this step two scenarios are possible: *i)* the points from the projected pattern are integrated in the global coordinate system and the

reference structure is updated from the reobserved distances between points, *ii)* both the observed structure and the 3-D pattern are stored and the reference structure is computed at the end of acquisition before integrating all frames in the global coordinate system. In this last case, the global coordinate system is linked to the view where the projected surface of the triangle is maximum. To make these two scenarios mostly equivalent, the first view that is used to bootstrap the positioning process is captured with the sensor viewpoint nearly align with the normal of the reference triangle.

The main source of error in the global coordinate system obviously arises from the sensor positioning error. This error depends on the accuracy of the reference points relative to their distances. In order to assess the actual measurement error, a planar section was scanned to the limits of visibility of a reference triangle whose sides were less than 100 *mm*. This led to a surface of nearly 450 *mm* wide and the uncertainty along the plane normal equal to 0,8 *mm*. Figure 4 illustrates this empirical evaluation.

6. Image processing and 3-D point computing

There are three objectives at the image processing level: identify isolated reference points, extract the laser trace position, and discriminate between the two sections of the crosshair. These can be made simple or very complex depending on the targeted precision. Estimating point or trace positions more accurately than 1/8th to 1/10th of a pixel would require a more sophisticated approach that takes into account different phenomena such as lag depicted in Figure 5. One can see that the peak distributions are not symmetrical. To demonstrate the proof of concept, simple but efficient operators were used to detect and estimate the peak positions.

Isolated points are detected as small blobs in the image. The maximum pixel value within the blob is identified and the estimation of the peak center position is refined by computing the center of gravity (using intensity as a weight) in a smaller (5x5) centered window. The blob pixels are then inhibited to prevent from interferences with other points.

To detect the projected crosshair sections, a simple linear differential operator, (-1 -1 -1 0 1 1 1), is convolved along image lines and a peak is identified at the zero crossing of the derivative provided the intensity is above a threshold. When such a zero crossing is detected, linear subpixel interpolation is applied. The peak position is preferably detected perpendicularly to the line.

Depending on the camera (C_1 or C_2), the crosshair section is identified and segmented into an active and an inactive plane. Since the sensor configuration causes the inactive plane to be projected near the principal point, it also ensures that its projection will be nearly a straight line of known orientation. This property of the sensor facilitates the crosshair separation as follows. For each detected peak, a gradient operator is applied one pixel right to the peak in order to estimate the local orientation of the line. For camera C_1, the identified peak is then tagged as potentially belonging to the inactive section if the laser trace orientation is nearly 45 degrees in the image. In the right image, the inactive section is identified if the angle is nearly 135 degrees. The parameters of these straight lines are then computed using the tagged pixels and refined using a subset of these pixels within a band of 5 pixels following the first line estimation. All pixels in the band are then tagged as inhibited. The peak positions are stored to validate the 3D position estimated in the opposite image. All remaining peaks in the image are shape candidates.

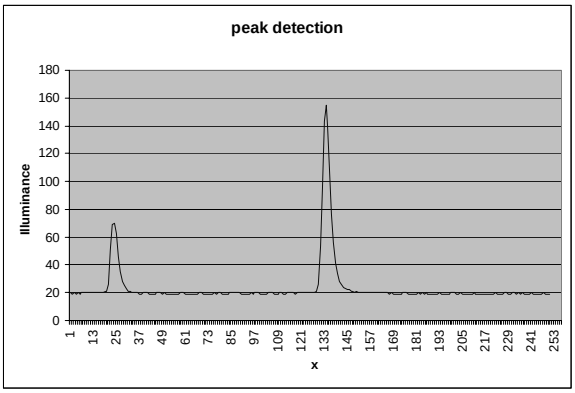

Figure 5. Intensity (irradiance) signal on a CCD line.

These candidates are confirmed after estimating the corresponding 3-D values using the calibrated plane equations and back projecting in the opposite image. Thus, a point is a validated 3-D point on the laser trace when it leads to a 3-D value within the working volume defined by the laser plane limits while its back projection in the opposite image is near (within a pixel) the inhibited branch of the projected crosshair.

Figure 6 illustrates an experiment made to assess the quality of peak detection. Using a planar object mounted on a translation stage and the sensor being fixed on a tripod, the plane was moved over a distance of 300 *mm* by steps of 5 mm. For each line in every image, the peak positions are detected and recorded. Then, the parameters of the colinearity equation are estimated [28]. Figure 6 (a) illustrates the fitted curve superimposed on the data. The discontinuity near position 47 indicates that no peak was detected on the line at this position. This corresponds to the passage of the crosshair center. Although the crosshair center could provide rich geometric information (e.g. local curvature), its accurate detection is problematic due to the

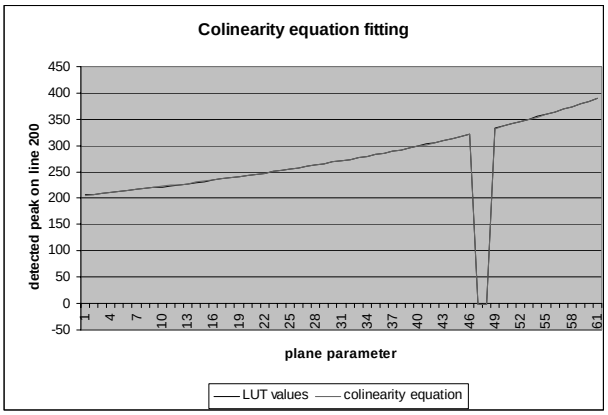

(a)

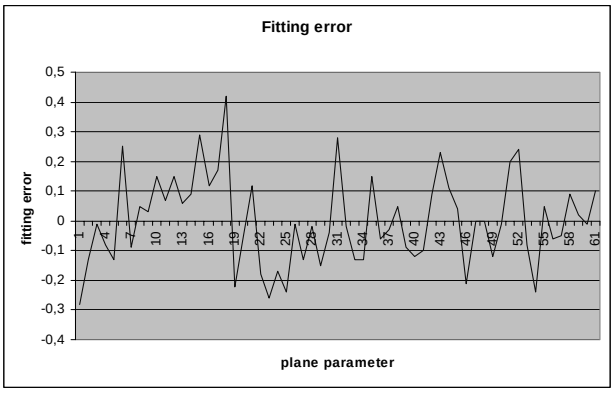

(b)

Figure 6. (a) Colinearity model equation fitting. (b) Peak position error with respect to the model.

strong irradiance at the local pixels. It is thus inhibited from the inactive section. The curve also shows a variation of 200 pixels over 300 *mm*; this corresponds to 1,5 *mm*/ pixel. Figure 6 (b) shows the error relative to the model. Typically, the average error is below 1/6 of a pixel; this corresponds to 250 microns.

Figures 7 and 8 illustrate the distributions of 3-D measurements (points) for two different objects. The points represent raw data; there is no filtering or processing. These figures are presented here to show that using only three points, it is possible to scan surface sections comparable to a full field sensor. However, there is the advantage to control the local sampling density and vary the incident viewing angle.

7. Conclusion

Although the fundamental characteristic of the sensor is the integration of sensor positioning and shape measurement, the sensor architecture presents many useful characteristics for measuring the geometry of objects. These include cooperating sensors for more robustness to detection and simplified pattern discrimination at the image processing level. The feasibility of a prototype has been demonstrated experimentally and some improvements are proposed. Adding a limited number of reference points would make it possible *i)* to reduce sensor position errors, *ii)* to ensure that a minimal number of reference points are always observed despite occlusions or pattern interferences, and *iii)* to significantly extend the covered surface.

An interesting perspective is to improve the sensor position estimates from the rigidity of the observed shape. This could be done using pattern registration. In this way, it is less crucial to accurately estimate the initial sensor location. The orientation of the crosshair makes it possible to benefit from pattern registration while the user naturally scans the surface by horizontal motion. The objective would be to reduce the error in the global coordinate system to a level that is closer to the error in the sensor coordinate system.

Acknowledgements

This work was performed under an NRCC contract. The author would like to thank Jacques Domey and Marc Rioux for their confidence and support. The author would also like to acknowledge the help of Sabry El-Hakim, Luc Cournoyer, Angelo Beraldin, François Blais and especially Guy Godin for many valuable discussions and comments.

References

[1] M. Levoy, K. Pulli, B. Curless, S. Rusinkiewicz, D. Koller, L. Pereira, M. Ginzton, S. Anderson, J. Davis, J. Ginsberg, J. Shade, and D. Fulk, “The Digital Michelangelo Project: 3D Scanning of Large Statues”, in *Proc. Siggraph ’2000*, 14 p., also available at http://www-graphics.stanford.edu/projects/mich/.

[2] Eois: Handy, http://www.eois.com

[3] Minolta: 3D1500, http://www.minolta.com/dp/3d1500

[4] H. Rushmeier and F. Bernardini, “Computing Consistent Normals and Colors from Photometric Data”, in *Proc. of the Second International Conference on 3-D Digital Imaging and Modeling*, Ottawa, Can., Oct. 1999, pp. 99-108.

[5] M. Petrov, A. Talapov, T. Robertson, A. Lebedev, A. Zhilyasev, and L. Polonskiy, “Optical 3D Digitizers: Bringing Life to the Virtual World”, *IEEE Computer Graphics and Applications*, Vol. 18, No. 3, 1998, pp. 28-37.

[6] Faro: Gold Faro arm, http://www.faro.com

[7] 3DScanners: ModelMaker, http://www.3dscanners.com

[8] Kréon Industrie: KLS series, http://www.kreon3d.com

[9] P. Hébert, J. Tremblay, F. Blais, H. Chotard, and S. Dyck, "Towards Flexible 3-D Digitizing Systems", in *Proc. of the IX European Signal processing Conference Eusipco'98*, Greece, Vol. III, Sep. 1998, pp.1281-1284.

[10] R. B. Fisher, A. Fitzgibbon, A. Gionis, M. Wright, D. Eggert, "A Hand-Held Optical Surface Scanner for Environmental Modeling and Virtual Reality", in *Proc. of Virtual Reality World '96*, Feb. 1996, Stuttgart, Ge. (also in technical report Dept. of AI, University of Edinburgh, DAI research paper No. 778, Dec 1995, 16 p.).

[11] T. D. Ditto and D. A. Lyon, "Moly, a Prototype Hand-Held 3D Digitizer with Diffraction Optics", *Optical Engineering*, Vol. 39, No. 1, Jan. 2000, pp. 69-78.

[12] Polhemus, Fastscan, http://www.polhemus.com/fastscan.htm

[13] Northern Digital: Optotrak, http://www.ndigital.com

[14] T. Koizumi and Y. Shirai, "Fundamental Study on the Development of the Close Range Photogrammetry without using any Control Points", in *Optical 3-D Measurement Techniques IV*, Gruen/Kahmen eds., Wichmann, 1997, pp. 393-399.

[15] M. Pollefeys, R. Koch, M. Vergauwen, and L. Van Gool, "Hand-held Acquisition of 3D Models with a Video Camera", in *Proc. of the Second International Conference on recent Advances on 3-D Digital Imaging and Modeling"*, Ottawa, Canada, Oct. 1999, pp. 14-23.

[16] G. Roth and A. Whitehead, "Using Projective Vision to Find Camera Positions in an Image Sequence", in *Proc. of Vision Interface '2000*, Montreal, Quebec, May 2000, pp. 225-232.

[17] R. W. Malz, "High Dynamic Codes, Self-Calibration and Autonomous 3D Sensor orientation: Three Steps towards Fast Optical Reverse Engineering Without Mechanical CMMs", in *Optical 3-D Measurement Techniques III*, Gruen/Kahmen eds., Wichmann, 1995, pp. 194-202.

[18] W. Niem and J. Wingbermuhle, "Automatic Reconstruction of 3D Objects Using a Mobile Monoscopic Camera", in *Proc. of the First International Conference on 3-D Digital Imaging and Modeling"*, Ottawa, Canada, Oct. 1997, pp. 173-180.

[19] J.-Y. Bouguet and P. Perona, "3D Photography using Shadows in Dual-Space Geometry", *International Journal of Computer Vision*, Vol. 35, No. 2, Nov. 1999, pp. 129-149.

[20] Immersion: LightScribe, http://www.immersion.com

[21] R. B. Fisher, A. P. Ashbrook, C. Robertson, N. Werghi, "A Low-Cost Range Finder using a Visually Located, Structured Light Source", in *Proc. of the Second International Conference on 3-D Digital Imaging and Modeling"*, Ottawa, Canada, Oct. 1999, pp. 24-33.

[22] M. Takatsuka, G. A. W. West, S. Venkatesh, T. M. Caelli, "Low-cost Interactive Active Monocular Range Finder", in *Proc. of the IEEE Conf. on Compter Vision and Pattern Recognition*, Fort Collins, CO, USA, Jun. 1999, pp. 444-449.

[23] N. A. Borghese, G. Ferrigno, G. Baroni, A. Pedotti, "Autoscan: A Flexible and Portable 3D Scanner", *IEEE Computer Graphics and Applications*, Vol. 18, No. 3, May/ Jun. 1998, pp. 38-41.

[24] P. Hébert, M. Rioux, "Toward a Hand-Held Laser range Scanner: Integrating Observation-based Motion Compensation", *in Proc. of SPIE: Three-Dimensional Image Capture and Applications*, Vol. 3313, San Jose, USA, 1998, pp. 2-13.

[25] A. Blake, D. McCowen, H. R. Lo, and P. J. Lindsey, "Trinocular Active Range-Sensing", *IEEE Transations on Pattern Analysis and Machine Intelligence*, Vol. 15, No. 5, May 1993, pp. 477-483.

[26] H. Hamdan, E. Hemayed, and A. Farag, "A Fast 3D Object Reconstruction using Trinocular Vision and Structured Light", in *Proc. of SPIE, Intelligent Robots and Computer Vision XVII: Algorithms, Techniques, and Active Vision*, Boston, USA, Vol. 3522, 1998, pp. 444-454.

[27] S. F. El-Hakim and N. J. Pizzi, "Multicamera Vision-Based Approach to Flexible Feature Measurement for Inspection and Reverse Engineering", *Optical Engineering*, Vol. 32, No. 9, Sep. 1993, pp. 2201-2215.

[28] J.-A. Beraldin, M. Rioux, F. Blais, G. Godin, and R. Baribeau, "Calibration of an Auto-synchronized Range Camera with Oblique Planes and Collinearity Equation Fitting", *Technical report ERB-1041*, NRC-CNRC, Nov. 1994, 36 p.

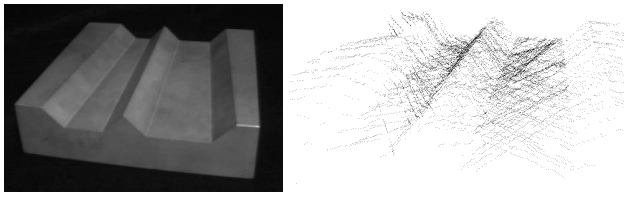

Figure 7. Measurement of a metal object (14104 points).

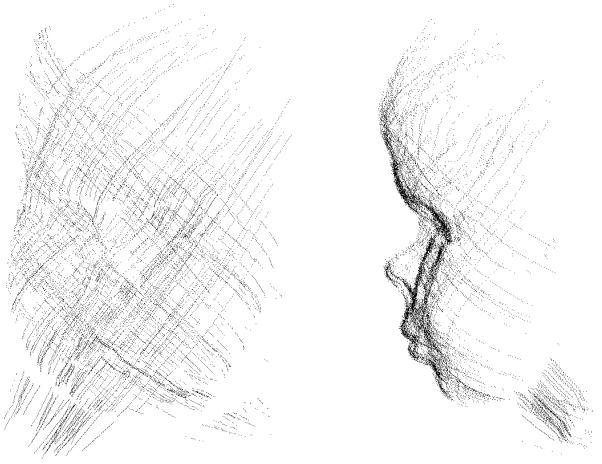

Figure 8. Front and side views of the spatial distribution of points for the mannequin head (17783 points).